Pure Appl. Chem., Vol. 80, No. 10, pp. 2091–2102, 2008.
doi:10.1351/pac200880102091

Development of new buffer layers for $Cu(In,Ga)Se_2$ solar cells*

Byung Tae Ahn‡, Liudmila Larina, Ki Hwan Kim, and Soong Ji Ahn

Department of Materials Science and Engineering, Korea Advanced Institute of Science and Technology, Daejeon 305-701, South Korea

Abstract: Recent progress in the field of $Cu(In,Ga)Se_2$ (CIGS) thin film solar cell technology is briefly reviewed. New wide-bandgap $In_x(OOH,S)_y$ and $ZnS_x(OH)_yO_z$ buffers for CIGS solar cells have been developed. Advances have been made in the film deposition by the growth process optimization that allows the control of film properties at the micro- and nanolevels. To improve the CIGS cell junction characteristics, we have provided the integration of the developed Cd-free films with a very thin CdS film. Transmittances of the developed buffers were greatly increased compared to the standard CdS. $In_x(OOH,S)_y$ buffer has been applied to low-bandgap CIGS devices which have shown poor photovoltaic properties. The experimental results obtained suggest that low efficiency can be explained by unfavorable conduction band alignment at the $In_x(OOH,S)_y$/CIGS heterojunction. The application of a wide-gap $Cu(In,Ga)(Se,S)_2$ absorber for device fabrication yields the conversion efficiency of 12.55 %. As a result, the $In_x(OOH,S)_y$ buffer is promising for wide-bandgap $Cu(In,Ga)(Se,S)_2$ solar cells, however, its exploration for low-bandgap CIGS devices will not allow a high conversion efficiency. The role played by interdiffusion at the double-buffer/CIGS heterojunction and its impact on the electronic structure and device performance has also been discussed.

Keywords: solar energy conversion; CIGS; thin film solar cells; Cd-free buffer layer; chemical bath deposition.

INTRODUCTION

$Cu(In,Ga)Se_2$ (CIGS) thin film semiconductors have bandgaps near the optimum value of terrestrial solar energy conversion, 1–1.7 eV. These chalcopyrite compounds are direct bandgap semiconductors which minimize the requirement for long minority carrier diffusion lengths. Such p-type semiconductors with high absorption coefficient are the promising absorbing materials for thin film photovoltaic technology.

When manufacturing thin film solar cells based on CIGS absorber layer, one of the critical components is the buffer layer which is positioned between CIGS absorber and ZnO window layer. Conventional CIGS solar cells typically comprise n-type CdS film serving as the buffer layer. These chalcopyrite compounds can be paired with CdS to make efficient p-n-type heterojunction solar cells because they have compatible lattice structures with acceptable lattice mismatches, and favorable differences of electron affinities. Thin film solar cells based on CIGS absorber layer and CdS buffer layer

*Paper based on a presentation at the International Conference and Exhibition "Molecular and Nanoscale Systems for Energy Conversion" (MEC-2007), 1–3 October 2007, Moscow, Russia. Other presentations are published in this issue, pp. 2069–2161.
‡Corresponding author

prepared by chemical bath deposition (CBD) have been a subject of intensive investigations for many years. Such devices are well known and have been the topic of numerous publications [1–7]. The state of the art in this technology is reviewed in [1].

The performance of CIGS photovoltaic devices has been optimized by adjusting the interface structure parameters. Employing the co-evaporation of Cu, In, Ga, and Se elements through a three-stage process and CBD CdS buffer layer, CIGS-based solar cells have achieved a high-energy conversion efficiency level of 19.5 % on a laboratory scale [3]. However, from environmental standpoint, the replacement of CdS is demanded for commercial production of CIGS cells. Due to this problem, considerable interest has recently been directed toward fabrication of Cd-free buffer layers for CIGS solar cells [8–20].

The other critical problem that faces the designers of CIGS solar cells involves the necessity to improve the light energy collection efficiency of the device. CdS buffer layer prepared by CBD is recognized as a superior buffer material for CIGS solar cells. However, the CIGS solar cells of the conventional art had the problem of undesired low CdS bandgap. The short wavelength response of CIGS solar cell is limited by low CdS bandgap of around 2.4 eV. As can be appreciated, the buffer layer for CIGS thin film solar cells must be transparent to the solar spectrum in order to provide the maximum of the light energy collection ability of the solar cells.

Prior efforts in development of such devices have generally been directed to wide-bandgap semiconductor materials. So far, several sulfide and selenide compounds such as ZnS, ZnSe, Zn(OH,S), Zn(OH,Se), and $In(OH,S)_x$ In_2S_3, $In_x(OOH,S)_y$ are possible alternative Cd-free materials for CIGS buffers [7–22]. These II–VI group compound semiconductors have relatively great energy bandgaps. The value of bandgap can be varied with the chemical composition of the film in the range between 2.0 and 3.7 eV. CIGS solar cells that use ZnS(O,OH) buffer layer grown by using CBD technique exhibit conversion efficiency up to 18.5 % [11,12]. Recently, the efficiency of approximately 14 % has been achieved for large-scale $Cu(In,Ga)(S,Se)_2$ (CIGSS) solar cells based on $Zn(Se,OH)/Zn(OH)_2$ and $Zn(O,S,OH)_x$ buffer layers [16,21]. Cd-free CIGS cells are relatively efficient. However, the efficiency of Cd-free CIGS cells is not high enough to compete with the exceptional efficiency of CIGS cells that employ Cd compound buffer. The advantages of the CdS buffer layer can be explained by a favorable conduction-band alignment at the CdS/CIGS heterojunction and compatible with CIGS lattice structure [4–6]. Recently, excellent results have been attained for thin film CIGS solar cells utilizing the mixed metal compound ($Cd_{1-x}Zn_xS$) buffer layer formed by CBD [22,23]. An efficiency of 19.52 % achieved in such cells is presently the highest known efficiency reported for a thin film solar cell [23].

For this purpose, we have been studying to find new buffer materials to replace the CdS buffer layer. In this paper we review some recent research conducted in our laboratory.

NEW BUFFER LAYERS FOR CIGS SOLAR CELLS

New wide bandgap Cd-free buffer layers have been developed in our laboratory. The buffer layers were grown by CBD method on either indium tin oxide (ITO) substrates or CIGS absorbers. The composition of CIGS absorber was adjusted as $Cu_{0.9}(In_{0.7}Ga_{0.3})Se_{2.1}$. The details of the evaporation procedure for the CIGS absorbers have been described in our publication [24]. The film that was grown from a chemical bath employed zinc sulfate as the metal ion source is referred to as Zn-based film. The film that was grown from a chemical bath employed indium chloride as the metal ion source, and is henceforth referred to in this investigation as In-based film. In view of the foregoing, we also have designed a buffer structure wherein the buffer layer has a desirable optical transmittance, while simultaneously having a favorable impact of the CdS on the electronic structure of the buffer/CIGS heterojunction. The above general purpose was accomplished by formation of a high-quality CdS thin film and In- or Zn-based film of the buffer being deposited in sequence on substrate.

In-based layers were deposited from the acetic aqueous solution containing indium(III) chloride and thioacetamide. Zn-based and CdS films were grown from the alkaline aqueous solutions. The al-

kaline aqueous solutions employed zinc sulfate, cadmium sulfate, and thiourea as zinc, cadmium, and sulfide ion sources, respectively. CBD processing parameters were optimized to improve the film quality and exclude the creation of morphology defects. The optimized deposition procedures have been described previously in detail [15,25].

The growth processes of In- and Zn-based by CBD are more complicated than that of CdS film. In particular, it is evident that there exists a large variety of conditions by which $In(OH)_3$, In_2O_3, or In_2S_3 can be deposited concurrently. The chemical composition of a metal compound film can be conveniently controlled by varying the CBD processing parameters. This possibility opens the wide opportunity to match the bandgap of metal compound films to the solar spectrum. In spite of the many research papers on the subject [17–20], the molecular formulas of the compounds deposited as thin film have not been well defined. The clarification of the composition, the structure, and the optical properties of CBD films of metal compounds are of great importance in connection with their use as buffer layers in thin film solar cells.

SURFACE MORPHOLOGY AND GROWTH KINETICS

We have studied the growth kinetics for all the developed buffer layers. The film thickness as a function of deposition time was estimated by scanning electron microscopy (SEM) measurements. The thickness of the film was shown to be strongly influenced by the deposition time and obeys linear dependence.

First, we have studied the evolution of CdS film morphology with film thickness. The morphology was shown to be strongly influenced by the film thickness. Optimized CBD process has been found to give uniform CdS coverage on either ITO or CIGS substrates with controllable thickness down to approximately 25 nm.

However, the CBD process for growth of Zn- and In-based films is more complicated than that of CdS film due to the difference in the values of solubility products. And lattice constant mismatch is likely to affect the film morphology and the coverage quality. SEM studies have shown that a good adhesive Zn-based film with tightly connected grain structure can be fabricated under optimized bath condition only with a thickness up to 60 nm (Figs. 1a-1, 1a-2). The increased film thickness results in defective films with cracks (Figs. 1b-1, 1b-2).

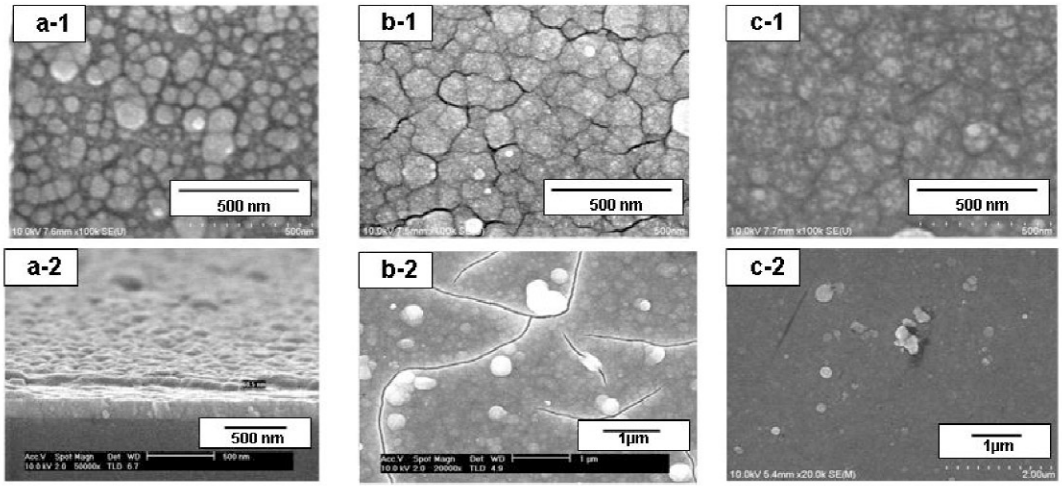

Fig. 1 SEM plane image (a-1) and tilt image (a-2) of the Zn-based film grown on ITO substrate with a thickness of 60 nm. SEM plane images (b-1, b-2) of the Zn-based film grown on ITO substrate with a thickness of 120 nm. SEM plane images (c-1, c-2) of the Zn-based film grown on ITO substrate by using the three-runs deposition process with a thickness of 130 nm.

The In-based film grown for 15 min exhibited a tightly connected dispersive grain structure with good adhesion to the substrates (Figs. 2a-1, 2a-2, 2a-3). When the deposition time increased, the individual grains formed a chaotic porous structure, which resulted in the porous film with bad adhesion to the substrates (Figs. 2b-1, 2b-2, 2b-3).

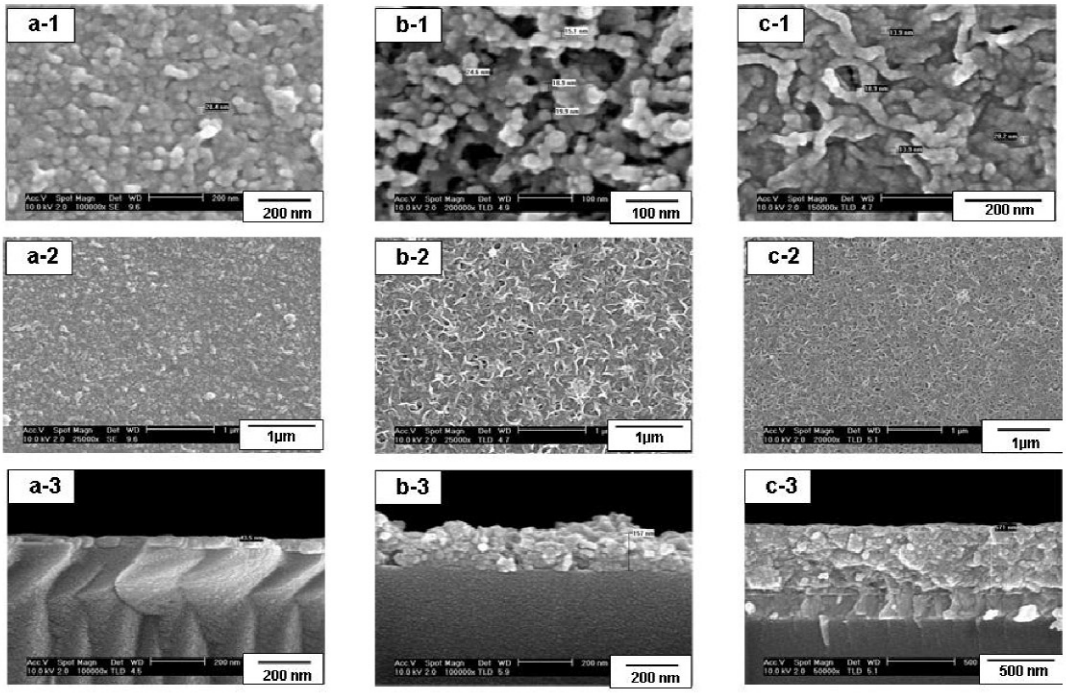

Fig. 2 SEM plane image (a-1, a-2) and cross-sectional image (a-3) of the In-based film grown on glass substrate for 15 min with a thickness of 40 nm. SEM plane image (b-1, b-2) and cross-sectional image (b-3) of the In-based film grown on glass substrate for 30 min with a thickness of 160 nm. SEM plane image (c-1, c-2) and cross-sectional image (c-3) of the In-based film grown on glass substrate by using the three-runs deposition process with a thickness of 570 nm.

The application of the multi-run deposition process enabled the success of the thickness growth of both types of films—Zn- and In-based. Zn-based buffer layer was grown under optimized CBD parameters by using sequential deposition of three very thin films on the substrate. In this way, high compact film structure was formed with a uniform covering of ITO substrate as well as the CIGS (Figs. 1c-1, 1c-2). SEM studies have shown that three-runs deposition allows the formation of a good adhesive In-based film with worm-shaped grains (Figs. 2c-1, 2c-2, 2c-3). The films with a thickness up to 500 nm exhibited a uniform covering of ITO substrate as well as glass. No cracking or peeling was observed in the films (Figs. 2c-1, 2c-2, 2c-3).

Finally, we have provided the integration of the Zn- or In-based film with a very thin CdS film to improve the CIGS cell junction characteristics. The developed double buffer layer comprises two layers deposited in a selected sequence on a substrate. Initially, about 20–40-nm-thick CdS film was deposited onto the surface of substrate, then about 60–200-nm-thick Zn- or In-based film was formed over CdS film. The same deposition procedure for growth of both layers of Zn- and In-based film was applied for forming double buffer layers. A homogeneous and pinhole-free double buffer layer was formed to a thickness within the range of 80–200 nm. Figures 3 and 4 provide the excellent illustration of the morphology for both double buffers—In-based/CdS and Zn-based/CdS.

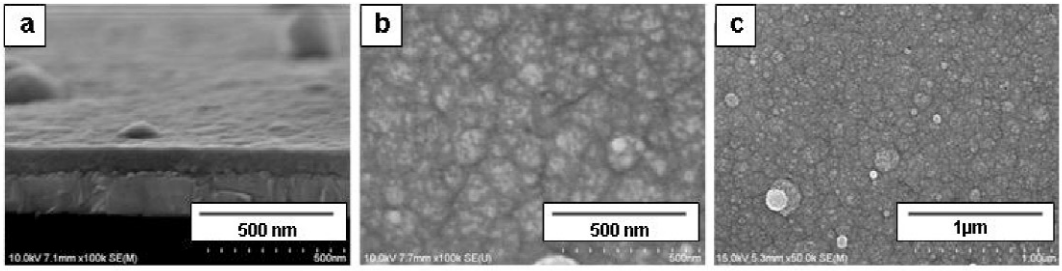

Fig. 3 SEM tilt image (a), and SEM plane image (b, c) of the Zn-based/CdS double buffer layer deposited on ITO substrate with a thickness of around 95 nm by using three-runs deposition process. CdS film was deposited on the surface of substrate with a thickness of around 25 nm.

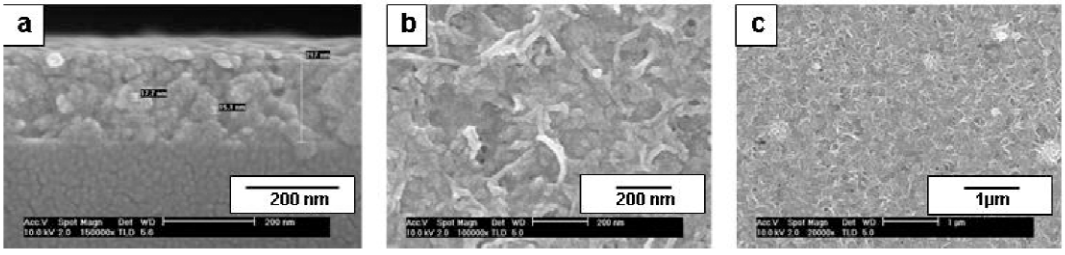

Fig. 4 SEM cross-sectional image (a), and SEM plane images (b, c) of the In-based/CdS double buffer layer deposited on Corning glass substrate with a thickness of around 215 nm by using two-runs deposition process. CdS film was deposited on the surface of substrate with a thickness of around 25 nm.

The growth kinetics and morphology of Zn- and In-based films was shown to be strongly influenced by the substrate nature. The above-mentioned results are in complete agreement with the predictions of the solution growth process [26].

In summary, we have succeeded in the growth of high-quality Zn- and In-based films through the optimization of CBD parameters and the use of the multi-run deposition. Advances have been made in the formation of the double buffer layer through the improvement of the individual layer surface properties and its control at the micro- and nanolevels.

STRUCTURE AND COMPOSITIONAL ANALYSES

The X-ray diffraction (XRD) pattern of the In-based film shows well-defined peaks, suggesting a high crystallinity of the film. By the combination of the X-ray photoelectron spectroscopy (XPS) and XRD we have shown the existence of the InOOH and In_2S_3 phases in the In-based film [15]. The annealing of the film above 500 °C in N_2 leads to the dehydration of the InOOH phase into the In_2O_3 phase. The result indirectly confirms the existence of an InOOH phase in the as-grown film. In the structural analysis summary, the In-based films contain In_2S_3 and InOOH phases and the overall chemical formula can be written as $In_x(OOH,S)_y$. The value of the In/S atomic ratio in the film suggests that the film consists of about 75 % In_2S_3 and about 25 % InOOH.

The XRD studies of as-deposited Zn-based films have indicated that the developed buffer layer possesses an amorphous structure. Auger sputter depth profile for Zn-based/CIGS interface revealed that the developed Zn-compound film can be described as the quaternary compound $ZnS_x(OH)_yO_z$ on the surface and as ZnS throughout the interface.

The elemental and chemical state identification of the double buffer layer formed of a first semiconductor CdS which is deposited in a thin film of about 25 nm on CIGS absorber, and a second ZnS

film was provided. Auger data have shown that the Zn-based/CdS/CIGS interface region does not consist of two abrupt interfaces, but it was a highly intermixed region with gradually changing composition. The Zn/S and O/Zn-S atomic ratios yield the surface ZnS and $Zn(OH)_2$ content of around 84 and 16 %, respectively. The estimated ZnS content ranges in the film from 98 % in the surface area to 57 % throughout the CdS/CIGS interface while CdS content ranges from 2 % in the vicinity of surface to 43 % throughout the CdS/CIGS interface. Finally, the film can be characterized as the ternary compounds $ZnS_x(OH)_y$ and $Zn_xCd_{(1-x)}S$ on the surface and throughout the buffer layer/CIGS interface, respectively.

It is well known that the band alignment is influenced by bandgaps of CIGS and buffer layer, and by the impact of intermixing effect at the buffer/CIGS interface. Taking into account the above-mentioned, we expect that a high intermixing will strongly influence the conduction-band offset (CBO) and Cd impact will decrease the CBO at the double buffer/CIGS interface compared to the large CBO for a single ZnS buffer.

OPTICAL ANALYSES

Figure 5a compares the optical transmittance spectra of the $In_x(OOH,S)_y$ and CdS films. The optical transmittance of $In_x(OOH,S)_y$ film is higher than that of the reference CdS film, approaching on the order of 90 % in the 550–420 nm wavelength range. An increase in optical transmittance of the $In_x(OOH,S)_y$ film of 27.9 % in the spectral range of 380–600 nm compares to the standard CdS film is achieved. As a result, the application of $In_x(OOH,S)_y$ film as a buffer layer for CIGS solar cells can provide the effective collection of the incident light in the short wavelength region of solar spectra. The absorption coefficient was derived from the measurements of the specular reflection, and the transmittance spectra of the $In_x(OOH,S)_y$ films [27]. We have shown that both types of transitions, direct and indirect, are observed in the film. It is considered that the direct and indirect bandgap of the $In_x(OOH,S)_y$ film is close to 3.5 and 2.1 eV, respectively. The estimated value of indirect bandgap is well fitted to that of In_2S_3 [28], but the value of the direct bandgap does not fit to previously known values and is believed to be originated from the InOOH phase. The difference in the direct bandgap between $In_x(OH)_yS_z$ and $In_x(OOH,S)_y$ indicates that the previously reported $In_x(OH)_yS_z$ films do not contain an InOOH phase [17,18].

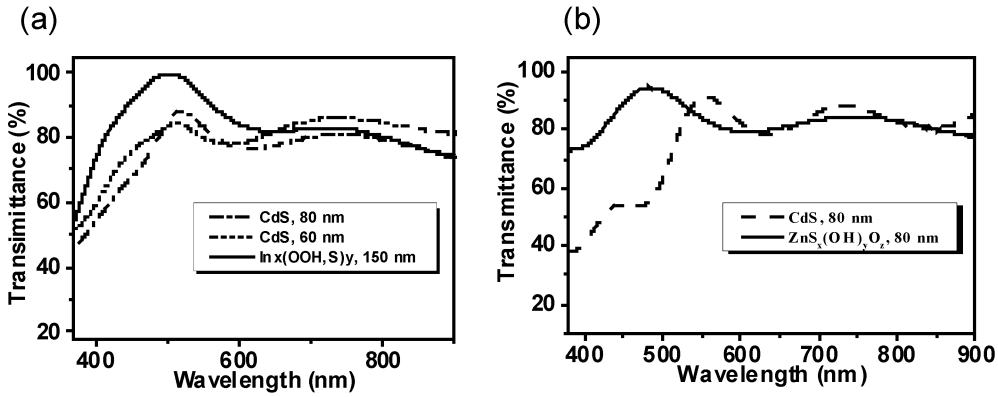

Fig. 5 (a) Optical transmittance spectra of the $In_x(OOH,S)_y$ and CdS films deposited on ITO substrates. (b) Optical transmittance spectra of CdS and $ZnS_x(OH)_yO_z$ films with the same thickness deposited on ITO substrates.

Figure 5b compares the optical transmittance spectra of a 80-nm-thick film of CdS and $ZnS_x(OH)_yO_z$ film with the same thickness. Referring now to Fig. 5b, we have shown that the absorption edge of the $ZnS_x(OH)_yO_z$ film shifts to a short wavelength side compares to the standard CdS film. An increase in optical transmittance of the $ZnS_x(OH)_yO_z$ film of 29.4 % in the spectral range of 380–600 nm compares to the standard CdS buffer is achieved.

In order to form controlled transmittance of double layers, the thicknesses of CdS film of the double buffer layer were varied. Figure 6a represents the optical transmittance spectra of a 80-nm-thick film of $ZnS_x(OH)_yO_z$ and the CdS films with different thickness. It is seen that the absorption edge of $ZnS_x(OH)_yO_z$ film shifts to a short wavelength side compared to CdS film as the thickness of CdS film exceeds 25 nm.

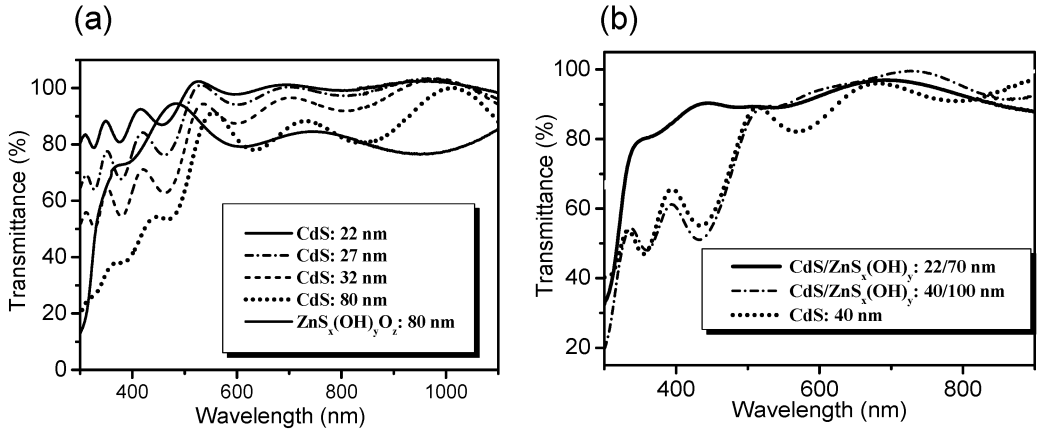

Fig. 6 (a) Optical transmittance spectra of the CdS films with different thickness and 80-nm-thick film of $ZnS_x(OH)_yO_z$ grown on ITO substrates. (b) Optical transmittance spectra of the $ZnS_x(OH)_y$/CdS double buffer layers and the CdS film grown on ITO substrates.

Figure 6b presents the excellent illustration of the optimized result to obtain the desirable optical transmittance spectra of the double buffer layer. It is seen that the optical transmittance of the double buffer layer is higher than that of the standard CdS buffer. As a result of the design optimization, an increase in optical transmittance of 24.9 % in the spectral range of 380–600 nm compared to the reference CdS layer was achieved.

The same optimization procedure was applied to growth of $In_x(OOH,S)_y$/CdS double buffer layer with high optical transmittance. Referring now to Fig. 7, we have shown that absorption edge of $In_x(OOH,S)_y$/CdS double buffer is shifted to a short wavelength side compared to the reference CdS film. And its optical transmittance is significantly higher than that of the standard CdS buffer.

Finally, by optimization of the double layer design we have formed buffer layers which enabled the transmission of the short wavelength of the solar spectrum for CIGS adsorption. Thus, we have succeeded in the growth of buffer layers, which can provide the maximum of the energy collection ability for CIGS thin film solar cell and also have a favorable Cd impact on its electronic structure.

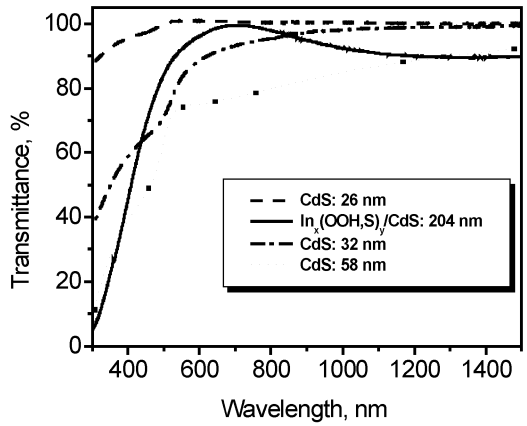

Fig. 7 Optical transmittance spectra of the $In_x(OOH,S)_y$/CdS double buffer layer and the CdS films with different thickness grown on Corning glass substrates.

PHOTOVOLTAIC PROPERTIES

We have fabricated CIGS solar cells of the conventional art by using the co-evaporation of Cu, In, Ga, and Se elements through a three-stage process. A Ga/(Ga + In) atomic ratio in CIGS absorbers was adjusted to be 0.3, which corresponds to bandgap of 1.12 eV. In our laboratory the energy conversion efficiency level of 18.37 % has been achieved, and the current–voltage characteristics of the photovoltaic devices are given in Fig. 8.

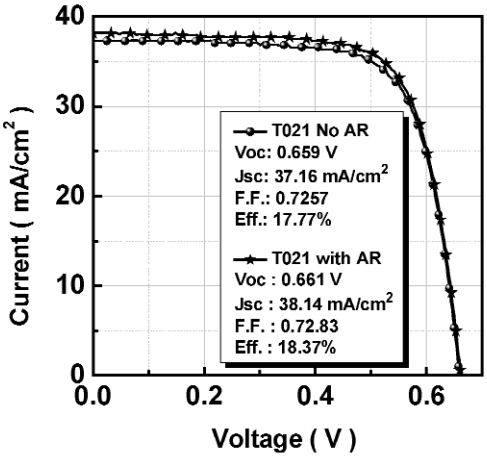

Fig. 8 *J–V* curves for CIGS solar cells with the CBD CdS buffer under AM 1.5 illumination.

The developed $In_x(OOH,S)_y$ buffer has been applied to solar cell as alternative for the standard CdS/CIGS device configuration. A set of CIGS solar cells utilizing the $In_x(OOH,S)_y$ buffer was fabricated. A standard CIGS cell with the CBD CdS buffer was prepared as a reference. CIGS cells were characterized by current–voltage and quantum efficiency (QE) measurements.

The devices that utilized $In_x(OOH,S)_y$ buffer layers have shown poor photovoltaic properties. The reference solar cell exhibited efficiency of 16.63 %, while the efficiency of the cell based on the $In_x(OOH,S)_y$/CIGS heterojunction was estimated to be only 3.39 %. The current–voltage curves of both solar cells under AM 1.5 illumination are given in Fig. 9a. The devices have demonstrated very similar

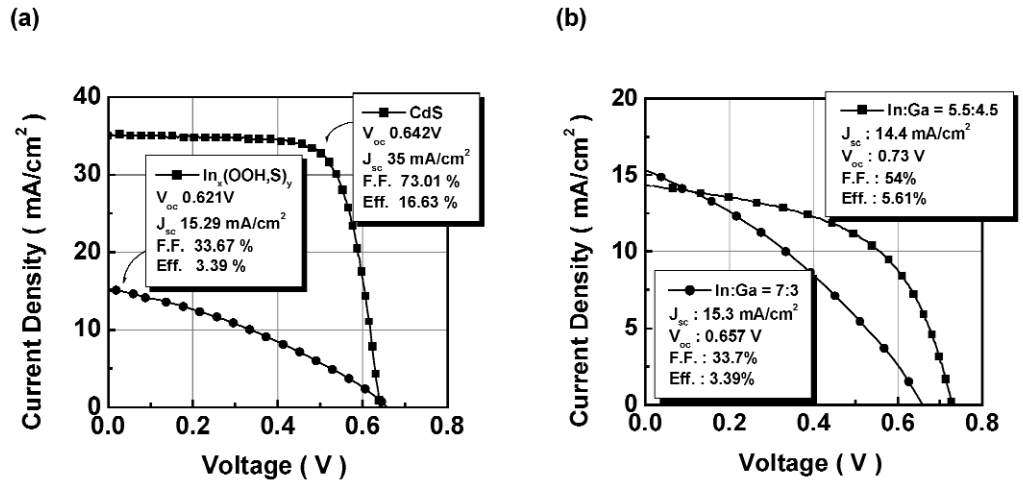

Fig. 9 *J–V* curves obtained under AM 1.5 illumination: (a) for CdS/CIGS and In$_x$(OOH,S)$_y$/CIGS heterojunction-based solar cells with the Ga/(In + Ga) ~ 0.3, and (b) for In$_x$(OOH,S)$_y$/CIGS heterojunction-based solar cells with the different Ga content in CIGS absorber.

values of the open-circuit voltage (V_{oc}), however, the short-circuit current (J_{sc}) dropped significantly in the CIGS solar cell that utilized In$_x$(OOH,S)$_y$ buffer. QE spectra for both devices show a considerable difference in response in a wavelength range of 500–1150 nm. The reference cell exhibits high QE, at the same time, the QE of the In$_x$(OOH,S)$_y$/CIGS heterojunction-based device decreases significantly as the wavelength increases.

A considerable QE decrease within the wavelength region of high In$_x$(OOH,S)$_y$ buffer transmittance points out that the carrier transport was hindered at the In$_x$(OOH,S)$_y$/CIGS interface. The problem of a low current collection is closely linked with impeded electron transport in the In$_x$(OOH,S)$_y$/CIGS structure, suggesting a spike barrier caused by the large conduction band offset at the In$_x$(OOH,S)$_y$/CIGS interface. As a result, this factor tends to decrease the conversion efficiency.

It has been reported elsewhere that the bandgap of the quaternary alloy system of Cu(In$_{1-x}$Ga$_x$)Se$_2$ varies with Ga content over a range of 1.04–1.67eV and the bandgap increases due to an upwards shift of the conduction band minimum [7,29,30]. To facilitate charge transfer across a In$_x$(OOH,S)$_y$/CIGS interface by lowering the energy barrier, we increased a value of Ga content in CIGS absorber. We have found that the increase in the solar cell conversion efficiency was consistent with the increase of Ga content in the CIGS absorber layer. The efficiency and V_{oc} raised to a maximum of 5.61 %, and 750 mV, respectively, for the Ga/(In + Ga) ratio of 0.45 (Fig. 9b). However, the benefit of increased Ga content was limited due to deterioration of the quality of CIGS absorber, leading to a poor device performance [1,6,31].

To facilitate electron transport across a In$_x$(OOH,S)$_y$/CIGS interface, the reverse bias was applied. Indeed, under the reverse bias condition, the In$_x$(OOH,S)$_y$/CIGS-based device has shown a considerable improvement of the QE. Furthermore, this effect was enhanced significantly with increase of the reverse bias, suggesting the voltage–dependence of the current collection efficiency. In fact, when the energy barrier is present, charge transport can be facilitated by a stronger junction field. However, the efficiency of the reference cell was not affected by the reverse bias, indicating a flat conduction band alignment at the CdS/CIGS interface. And as result, the favorable CBO leads to an unimpeded electron transport across the heterojunction. These findings are in line with the literature [5]. The application of the reverse bias to the device with high Ga content [Ga/(In + Ga) ~ 0.45] in CIGS absorber yields a better spectral response, but the reverse bias effect was substantially less than that in a low-bandgap CIGS

device. The experimental data obtained prove an unfavorable band offset at the $In_x(OOH,S)_y$/CIGS heterojunction.

To verify the conduction band offset, an XPS depth profile analysis of the ZnO/$In_x(OOH,S)_y$/CIGS interface structure was carried out. The measured value of CBO was found to be 1.0 eV at the $In_x(OOH,S)_y$/CIGS interface. Such a large CBO is consistent with the experimental results, described in the above paragraphs. Indeed, the estimated spike barrier is high enough to block the carrier transport across an $In_x(OOH,S)_y$/CIGS heterojunction, and to cause the sharp drop in the J_{sc} and fill factor (FF).

To overcome this problem, the pentenary alloy system $Cu(In,Ga)(Se,S)_2$ (CIGSS) was applied as a wide-gap absorber for device fabrication. The central R&D laboratory of Showa Shell Sekiyu K.K., Japan, has provided the CIGSS absorbers [21]. A standard CIGSS cell with the CBD CdS buffer was prepared as a reference. For comparison purposes, Fig. 10 represents the current–voltage curves of the reference CIGSS solar cell and the cell based on the $In_x(OOH,S)_y$/CIGSS heterojunction.

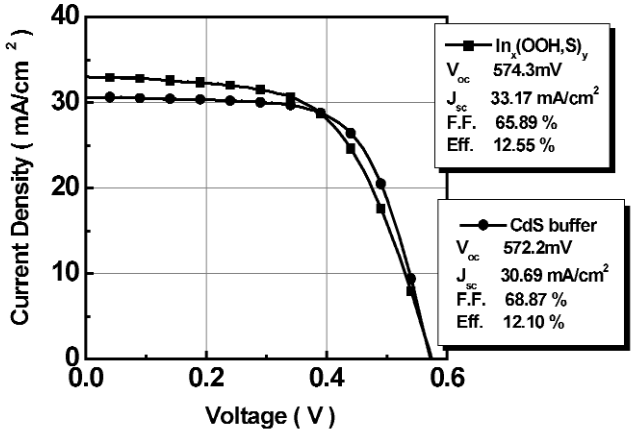

Fig. 10 *J–V* curves for CIGSS solar cells with the CdS and $In_x(OOH,S)_y$ buffer layers under AM 1.5 illumination.

The conversion efficiency of the CIGSS cell with the $In_x(OOH,S)_y$ buffer is 12.55 % with a J_{sc} of 33.17 mA/cm^2, V_{oc} of 574.3 mV, and FF of 65.89 % for an active area of 0.19 cm^2. The values of conversion efficiency and J_{sc} are higher than that in the reference cell (12.10 %, 30.69 mA/cm^2). Both devices have shown similar spectral responses in the long wavelength region. However, the short wavelength response in the CIGSS cell with the $In_x(OOH,S)_y$ buffer is higher compared to that in the reference cell. The strong short wavelength response can be assigned to high optical transmittance of the $In_x(OOH,S)_y$ buffer in the short wavelength region (see Fig. 5a).

CONCLUSION

We have succeeded in the growth of buffer layers, which could allow the maximum of the energy collection ability for CIGS thin film solar cells in the short wavelength region. The integration of developed $In_x(OOH,S)_y$ and $ZnS_x(OH)_y$ film with a very thin CdS film has been provided to improve the junction characteristics of CIGS devices. CIGS solar cells that employ the newly developed double buffer layer utilize a negligible quantity of hazardous material. The experimental results obtained suggest that the limitation of a J_{sc} that was found in low-bandgap CIGS devices can be explained by a large CBO at the $In_x(OOH,S)_y$/CIGS heterojunction. The application of a wide-bandgap CIGSS absorber and $In_x(OOH,S)_y$ buffer for device fabrication yields the energy conversion efficiency of 12.55 %. This efficiency is competitive with the best efficiency observed in CIGSS solar cells of the conventional art.

As a result, the developed $In_x(OOH,S)_y$ buffer layer is promising for wide-bandgap CIGSS solar cell application, however, its exploration for low-bandgap CIGS devices will not allow a high conversion efficiency. Our experimental results clearly show that the formation of the heterojunction is a key issue in the fabrication of high-efficiency CIGS solar energy conversion devices.

ACKNOWLEDGMENTS

The authors are grateful to the Center for Nanointerface Technology, KAIST for a partial supporting of this work. This work was also supported by the Korea Research Foundation Grant (KRF-2005-005-J09072).

REFERENCES

1. M. Turcu, O. Pakma, U. Rau. *Appl. Phys. Lett.* **80**, 2598 (2002).
2. N. G. Dhere. *Sol. Energy Mater. Sol. Cells* **90**, 2181 (2006).
3. M. A. Contreras, K. Ramanathan, J. A. Shama, F. Hasoon, D. L. Young, B. R. Egaas. *Prog. Photovolt. Res. Appl.* **13**, 209 (2005).
4. K. Ramanathan, M. Contreras, C. Perkins, S. Asher, F. Hasoon, J. Keane, D. Young, M. Romero, W. Metzger, R. Noufi, J. Ward, A. Duda. *Prog. Photovolt. Res. Appl.* **11**, 225 (2003).
5. M. Morkel, L. Weinhardt, B. Lohmuller, C. Heske, E. Umbach, W. Riedl, S. Zweigart, F. Karg. *Appl. Phys. Lett.* **79**, 4482 (2001).
6. G. Hanna, A. Jasenek, U. Rau, H. W. Schock. *Phys. Status Solidi A* **179**, R7 (2000).
7. K. Kushiya, Y. Ohtake, A. Yamada, M. Konagai. *Jpn. J. Appl. Phys*. **33**, 6599 (1994).
8. A. Ennaoui, S. Siebentritt, M. Lux-Steiner, W. Riedl, F. Karg. *Sol. Energy Mater. Sol. Cells* **67**, 31 (2001).
9. R. Bayon, C. Guillen, M. A. Martinez, M. T. Gutierrez, J. Herrero. *J. Electrochem. Soc.* **145**, 2775 (1998).
10. T. Nakada, M. Mizutani. *Jpn. J. Appl. Phys*. **41**, 165 (2002).
11. M. A. Contreras, T. Nakada, M. Hongo, A. O. Pudov, J. R. Sites. *Proc. 3rd World Conf. Photovoltaic Energy Conv.*, Osaka, Japan, 2LN-C-08 (2003).
12. R. N. Bhattacharya, M. A. Contreras, G. Teeter. *Jpn. J. Appl. Phys.* **43**, L1475 (2004).
13. N. Naghavi, R. Henriquez, V. Laptev, D. Lincot. *Appl. Surf. Sci.* **222**, 65 (2004).
14. Y. Tokita, S. Chaisitsak, A. Yamada, M. Konagai. *Sol. Energy Mater. Sol. Cells* **75**, 9 (2003).
15. L. Larina, K. H. Kim, K. H. Yoon, M. Konagai, B. T. Ahn. *J. Electrochem. Soc.* **151**, C789 (2004).
16. W. Eisele, A. Ennaoui, P. Schubert-Bischoff, M. Giersig, C. PettenKofer, J. Krauser, M. Lux-Steiner, S. Zweigar, F. Karg. *Sol. Energy Mater. Sol. Cells* **75**, 17 (2003).
17. C. H. Huang, S. S. Li, W. N. Shafarman, C.-H. Chang, E. S. Lambers, L. Rieth, J. W. Johnson, S. Kim, B. J. Stanbery, T. J. Anderson, P. H. Holloway. *Sol. Energy Mater. Sol. Cells* **69**, 131 (2001).
18. T. Nakada, M. Hongo, E. Hayashi. *Thin Solid Films* **431–432**, 242 (2001).
19. R. Bayon, J. Herrero. *Thin Solid Films* **387**, 111 (2001).
20. R. Bayon, J. Herrero. *Appl. Surf. Sci.* **158**, 49 (2000).
21. K. Kushiya, M. Tachiyaki, Y. Nagoya, A. Fujimaki, B. Sang, D. Okumura, M. Satoh, O. Yamase. *Sol. Energy Mater. Sol. Cells* **67**, 11 (2001).
22. R. N. Bhattacharya, K. Ramanathan, L. Gedvilas, B. Keyes. *J. Phys. Chem. Solids* **66**, 1862 (2005).
23. R. N. Bhattacharya, M. A. Contreras, B. Egaas, R. N. Noufi, A. Kanevce, J. R. Sites. *Appl. Phys. Lett.* **89**, 253503 (2006).
24. K. H. Kim, K. H. Yoon, J. H. Yun, B. T. Ahn. *Electrochem. Solid-State Lett.* **9**, A382 (2006).
25. L. Larina, K. H. Kim, K. H. Yoon, B. T. Ahn. South Korea Patent 10-0625082, Filed 25 October 2004, Issued 11 September 2006.

26. K. L. Chopra, S. R. Das. *Thin Film Solar Cells*, p. 225, Plenum Press, New York (1983).
27. J. I. Pankove. *Optical Processes in Semiconductors*, p. 93, Dover, New York (1987).
28. G. A. Kitaev, V. I. Duoinin, A. V. Ustyantseva, M. N. Belyaeva, L. G. Skorgakow. *Neorg. Mater.* **12**, 1760 (1976).
29. A. D. Katnani, G. Margaritondo. *Phys. Rev. B* **28**, 1944 (1983).
30. M. Gloeckler, J. R. Sites. *Thin Solid Films* **480–481**, 241 (2005).
31. W. N. Shafarman, R. Klenk, B. E. McCandless. *J. Appl. Phys.* **79**, 7324 (1996).